Journal of Non-Crystalline Solids 663 (2025) 123568

Contents lists available at ScienceDirect

Journal of Non-Crystalline Solids

journal homepage: www.elsevier.com/locate/jnoncrysol

High thermal stability of amorphous TiO_2 enhanced by OH

Benshun Ma [a,b,†], Xiao Chen [a,b,†], Jianing Wang [a,b], Wei Xu [a], Lijian Song [a], Meng Gao [a], Juntao Huo [a,b,*], Jun-Qiang Wang [a,b,*]

[a] CAS Key Laboratory of Magnetic Materials and Devices, and Zhejiang Province Key Laboratory of Magnetic Materials and Application Technology, Ningbo Institute of Materials Technology and Engineering, Chinese Academy of Sciences, Ningbo 315201, China
[b] Center of Materials Science and Optoelectronics Engineering, University of Chinese Academy of Sciences, Beijing 100049, China

ARTICLE INFO

Keywords:
Amorphous TiO_2
Thermal stability
Lunar ilmenite
Crystallization enthalpy
Activation energy

ABSTRACT

Amorphous titanium dioxide (A-TiO_2), a key component of lunar ilmenite's surface layer and a promising material for helium bubble encapsulation, plays a vital role in lunar resource utilization. This study focuses on its thermal stability, a critical factor for practical applications. A-TiO_2 is successfully synthesized via the sol-gel method, and its thermodynamic properties are systematically investigated using TG-DSC. It is found that hydroxyl groups enhance the thermal stability of A-TiO_2 at ambient temperature by forming hydrogen bond networks. Specifically, after 15 days of aging, hydroxyl-rich A-TiO_2 exhibit a crystallization enthalpy of 147.8 J/g, significantly larger than that of hydroxyl-free counterparts (110.2 J/g). Isochronal crystallization analysis reveals that the instantaneous A-TiO_2 after dehydration exhibits much lower crystallization activation energy (E_a = 321.1 kJ/mol) than the relaxed hydroxyl-free A-TiO_2 (E_a = 415.7 kJ/mol). This suggests that hydrogen bond network stabilize the amorphous structure of A-TiO_2. These findings are also helpful for understanding the long-time stability for the lunar amorphous TiO_2.

1. Introduction

Titanium dioxide (TiO_2), a versatile metal oxide semiconductor [1,2], plays a pivotal role in numerous applications, ranging from photocatalysis [3] and chemical sensing [4] to durable coatings [5,6] and advanced ceramics [7]. Its synthesis is well-established through various methods, including sol-gel processing [8,9], hydrothermal synthesis [10], and physical vapor deposition [11,12]. While crystalline phases like anatase, rutile, and brookite have been extensively studied, amorphous TiO_2(A-TiO_2)—with its disordered atomic structure and thermodynamic metastability—has recently emerged as a material of significant interest due to its unique properties [13,14]. For instance, Rodríguez-Páez et al. demonstrated its efficacy as an antibacterial agent [15], while Yuan Liu et al. showcased its exceptional electrochemical performance for lithium storage [16]. Additionally, T. Tarjányi et al. explored its surface interactions with biopeptides, underscoring its biomedical potential [17].

The most intriguing discovery comes from lunar soil analysis, where an A-TiO_2 layer was identified on ilmenite particles in Chang'e 5 samples [18]. This layer can encapsulate helium-3 bubbles—a finding with profound implications for lunar resource utilization [19–22]. However, it is amazing and puzzling that why the A-TiO_2 layer are so stable across billions of years. This is inconsistent with the metastable characters that are prone to crystallize [23,24]. It is found that due to long-term exposure to solar wind irradiation, hydroxyl groups tend to accumulate in the A-TiO_2 layer on the surface of lunar minerals [22,25–27]. A systematic investigation into the thermal properties of A-TiO_2 is urgently needed. Such research would not only advance our fundamental understanding of this material but also provide critical insights for developing efficient helium-3 extraction technologies, paving the way for sustainable lunar resource utilization [28].

In this study, A-TiO_2 was synthesized via the sol-gel method using tetrabutyl titanate (TBOT) as the precursor. The synthesized samples were characterized using scanning electron microscopy (SEM), transmission electron microscopy (TEM), X-ray diffraction (XRD), thermogravimetric-differential scanning calorimetry (TG-DSC), and fourier transform infrared diffuse reflectance spectroscopy (FTIR-DRIFTS) to analyze their structural, morphological, and thermal properties. Additionally, we investigated the kinetic behaviors, thermodynamic parameter evolution, and influencing factors of A-TiO_2. These

* Corresponding authors.
E-mail addresses: huojuntao@nimte.ac.cn (J. Huo), jqwang@nimte.ac.cn (J.-Q. Wang).
† These authors contribute equally.

https://doi.org/10.1016/j.jnoncrysol.2025.123568
Received 24 February 2025; Received in revised form 15 April 2025; Accepted 18 April 2025
Available online 6 May 2025

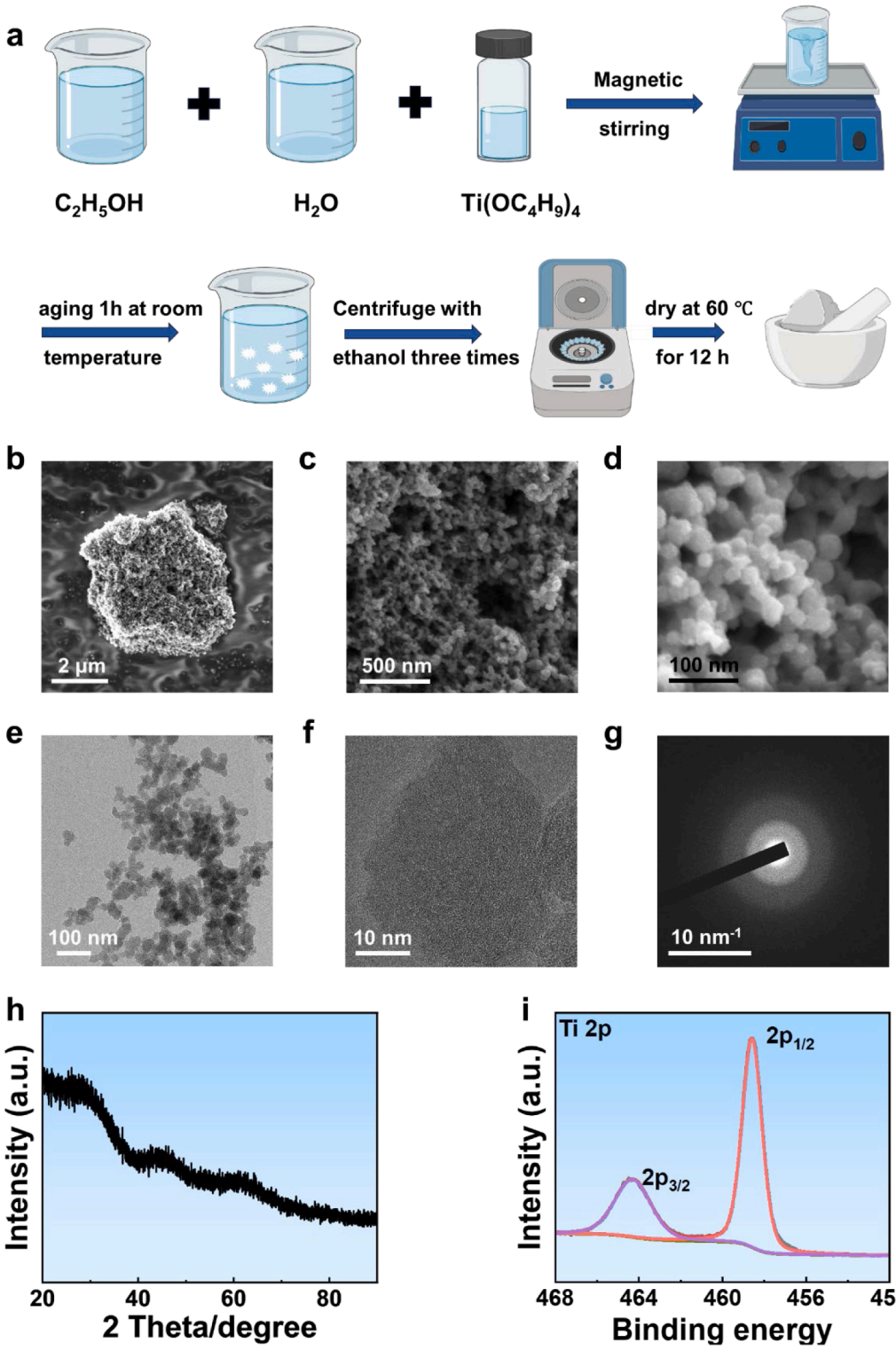

Fig. 1. (a) Preparation process diagram of A-TiO_2. (b-d) SEM images of A-TiO_2 with varying sizes, showcasing the transition from microscale to nanoscale within the same sample. (e-f) TEM images of A-TiO_2 with varying sizes. (g) SAED pattern of A-TiO_2, confirming its non-crystalline structure. (h) XRD pattern of A-TiO_2. (i) XPS spectrum of Ti 2p for the A-TiO_2 sample.

findings provide valuable insights into the material's properties, advancing its potential applications in advanced materials science and extraterrestrial resource utilization.

2. Material and method

2.1. Preparation of A-TiO_2

Tetrabutyl titanate (TBOT) was employed as the precursor for the synthesis of A-TiO_2 through the sol-gel method [29–31]. The reaction

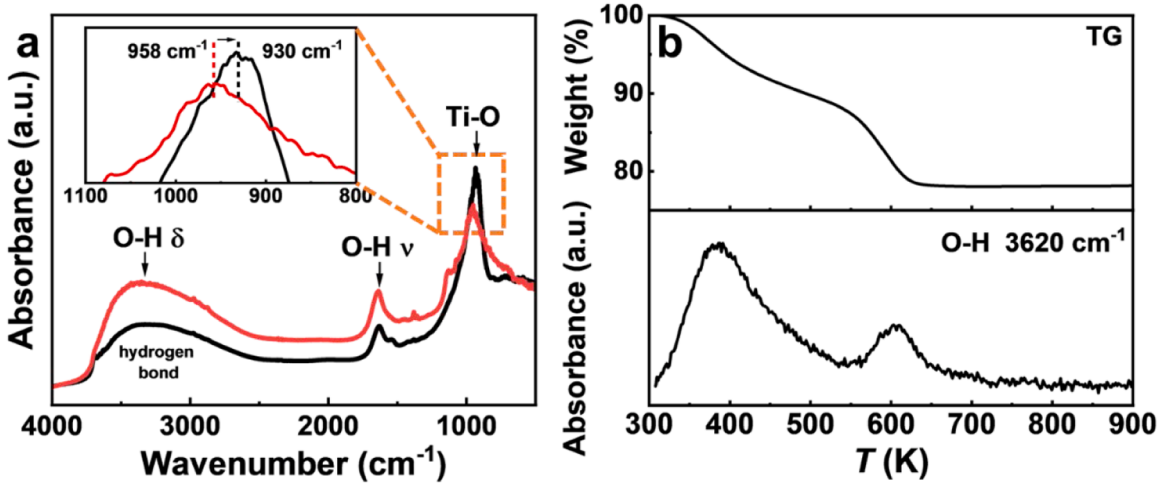

Fig. 2. (a) FTIR-DRIFT spectrum of the amorphous TiO_2 samples, covering the range of 400- 4000 cm^{-1}. Hydroxyl-rich sample (red) exhibit a stronger Ti-O bonding compared to the hydroxyl-lack sample (black). (b) TG-IR analysis of the sample: the upper panel shows the TG curve upon heating to 900 K, while the lower panel displays the infrared absorption spectrum at 3620 cm^{-1}, corresponding to the gases released during the heating process.

mechanism is described by the following equation:

$$Ti(OC_4H_9)_4 + 2H_2O \rightarrow TiO_2 + 4C_4H_9OH$$

Figure 1(a) is a schematic diagram of the sample preparation process. Initially, two solutions were prepared: Solution S1, consisting of 4 mL of $Ti(OC_4H_9)_4$ mixed with 100 mL of ethanol (C_2H_5OH), and Solution S2, comprising 100 mL of ethanol (C_2H_5OH) and 100 mL of deionized water (H_2O). Solution S2 was subjected to continuous magnetic stirring, while Solution S1 was introduced dropwise into Solution S2 at a controlled

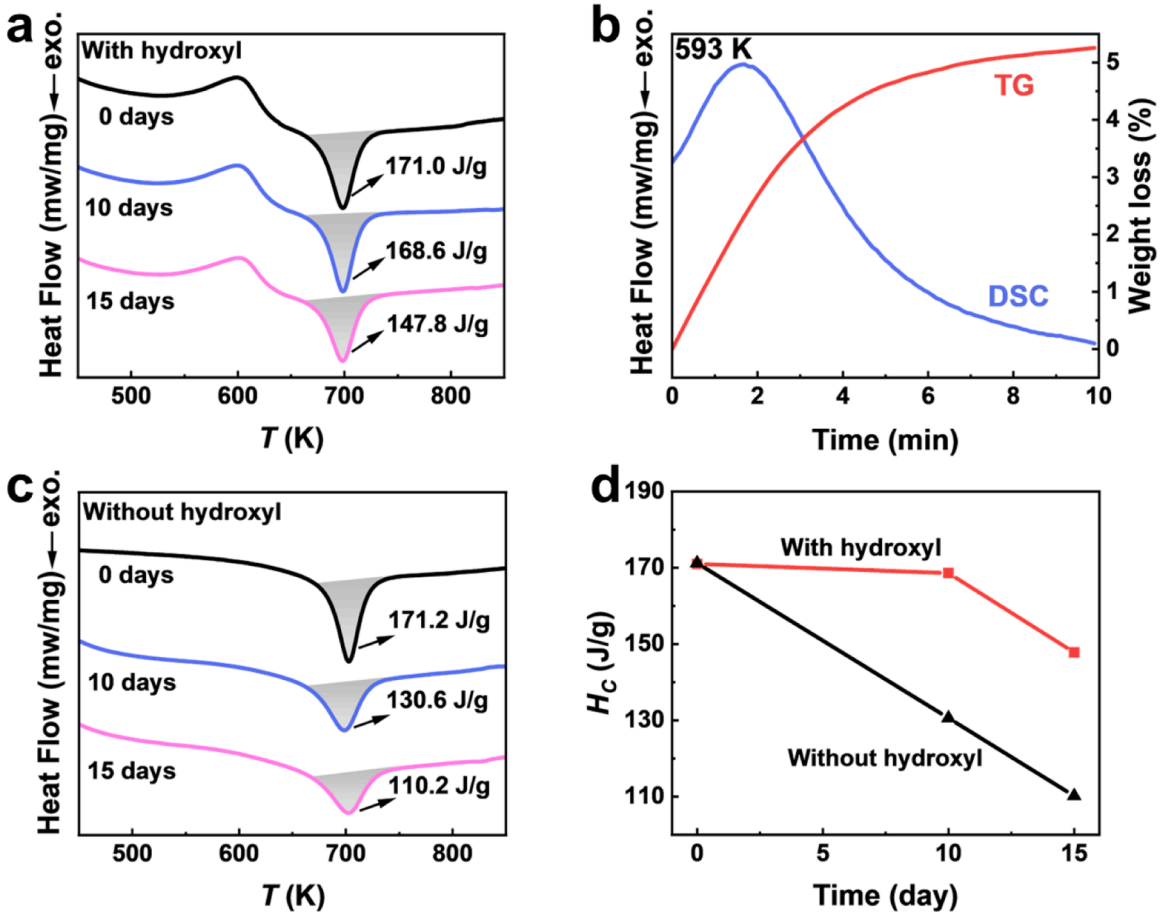

Fig. 3. (a) DSC curves and crystallization enthalpy of OH-containing samples aged for different durations: as-prepared sample (black curve), after 10 days (blue curve), and after 15 days (pink curve). (b) TG-DSC curves of the sample held at 593 K for 10 min: TG curve (red) and DSC curve (blue). The process involves heating the sample to 593 K and holding for 10 min to remove OH groups. (c) DSC curves and crystallization enthalpy of OH-free samples aged for different durations: as-prepared sample (black curve), after 10 days (blue curve), and after 15 days (pink curve). (d) Comparison of crystallization enthalpy over time for A-TiO_2 with and without OH groups: the OH-containing sample (red curve), and the OH-free sample (black curve).

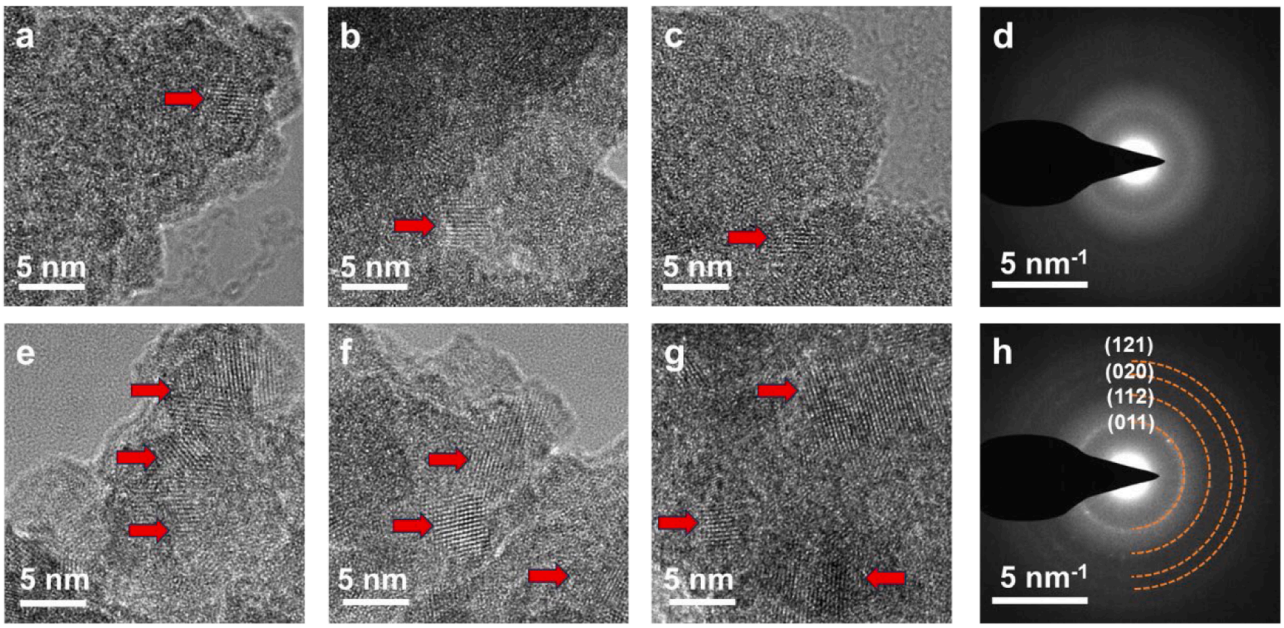

Fig. 4. (a-c) TEM images of the OH-containing sample after 15 days of aging. Red arrows indicate lattice fringes in regions where crystallization has initiated. (d) SAED pattern of the OH-containing sample after 15 days of aging. (e-g) TEM images of the OH-free sample after 15 days of aging. Red arrows highlight lattice fringes in regions showing initial crystallization. (h) SAED pattern of the OH-free sample after 15 days of aging.

rate of one drop per second. Upon completion of the dripping process, the mixture was allowed to stand at room temperature for one hour, during which the TiO_2 precursor precipitated from the solution. The resulting white precipitate was then suspended in ethanol and subjected to centrifugal washing three times to remove impurities. Following washing, the precipitate was dried in air at 333 K for 12 h.

The hydroxyl-free A-TiO_2 were prepared by annealing the samples in an argon atmosphere at 593 K for 10 min to remove OH groups and then cooled to room temperature. Finally, the sample was stored in a glove box to prevent contamination and ensure stability for further characterization and analysis.

2.2. Characterizations

The morphology and structure were observed by scanning electron microscopy (SEM, Thermo Scientific Verios G4 UC). The amorphous structure of the prepared samples was analyzed by transmission electron microscopy (TEM) observations on talos F200X (Thermo Scientific) operating at an acceleration voltage of 200 kV. The phase structures were determined by an X-ray diffraction (XRD) equipment (Bruker D8 ADVANCE) using Cu Kα radiation. To identify the nature of the bondings, the Fourier Transform Infrared Diffuse Reflectance Spectroscopy (FTIR-DRIFT) of the samples were measured with a Nicolet 6700 and collected in the frequency range of 400–4000 cm^{-1}. TG-FTIR-MS analysis of the samples were performed on an integrated analyzer (PerkinElmer) with a ramping rate of 10 K/min under N_2 flow. The thermal analysis for cross-linking process was carried out on TG-DSC (Netzsch STA 449) with a ramping rate of 5, 10, 15, 20 K/min under N_2 flow.

3. Results and discussion

Fig. 1(a) schematically illustrates the preparation process of A-TiO_2. Figs. 1(b-d) present SEM images of the synthesized A-TiO_2 at micro-to-nano scales, revealing that the A-TiO_2 particles consist of primary nanoparticles with an average size of ~20 nm, forming a nanoporous architecture. TEM images (Figs. 1e-f) demonstrate the amorphous structure of the sample, as evidenced by the absence of lattice fringes in HRTEM observations. The SAED pattern in Fig. 1(g) displays characteristic diffuse rings, further confirming the amorphous structure. The XRD profile (Fig. 1h) of the sol-gel-derived A-TiO_2 exhibits no distinct diffraction peaks, consistent with its non-crystalline nature and in agreement with TEM results. XPS analysis (Fig. 1i) reveals two well-defined Ti 2p peaks at 458.6 eV ($2p_{3/2}$) and 464.3 eV ($2p_{1/2}$), showing enhanced spectral symmetry. The 5.7 eV energy separation between these peaks matches the characteristic binding energy of Ti(IV) ions [32]. These comprehensive characterizations collectively confirm the successful synthesis of A-TiO_2 with structural homogeneity.

Fig. 2(a) displays the FTIR-DRIFTS spectrum of sol-gel-derived A-TiO_2 in the range of 400–4000 cm^{-1}. A distinct peak at 1600 cm^{-1} is attributed to the bending vibration of O—H groups. The absorption band between 3200 and 3600 cm^{-1} corresponds to O—H stretching vibrations. The presence of hydrogen bonds causes the absorption band to broaden, confirming the hydrophilic nature of A-TiO_2 [32–34]. In the low-wavenumber region (800–1000 cm^{-1}), characteristic Ti-O vibrational modes are observed, including stretching and bending vibrations of Ti-O-Ti and Ti-O-H bonds, which collectively define the structural framework of A-TiO_2 [32,35]. It is shown that the Ti-O peak shifts to lower frequency from 958 to 930 cm^{-1} after dehydration. This suggests that hydroxyl can strength the Ti-O bonding.

Fig. 2(b) presents the TG-IR analysis results. The TG curve shows a ~25 % mass loss between 300 K and 600 K, primarily due to desorption of physically absorbed water and decomposition of OH groups. Hydroxyl signals detected in the 300–450 K range correspond to weakly bound water (typically physically adsorbed water) with no direct chemical bonding to the material. Signals in the 500–650 K range originate from structural hydroxyl groups chemically bonded to the material. The TG-IR results further validate the hydrated nature of A-TiO_2 synthesized via the sol-gel method.

Fig. 3(a) displays the DSC curves of hydroxyl-containing A-TiO_2 after being stored for 10 days and 15 days. The curves (hydroxyl-containing sample) exhibit an endothermic peak at 600 K, consistent with TG-IR results, confirming hydroxyl desorption at this temperature. An exothermic peak at 700 K corresponds to crystallization, marking the phase transition from amorphous to crystalline TiO_2. The 10-day sample exhibits a crystallization enthalpy of 168.6 J/g, which is nearly identical to the initial sample's value (171.0 J/g), indicating minimal changes in

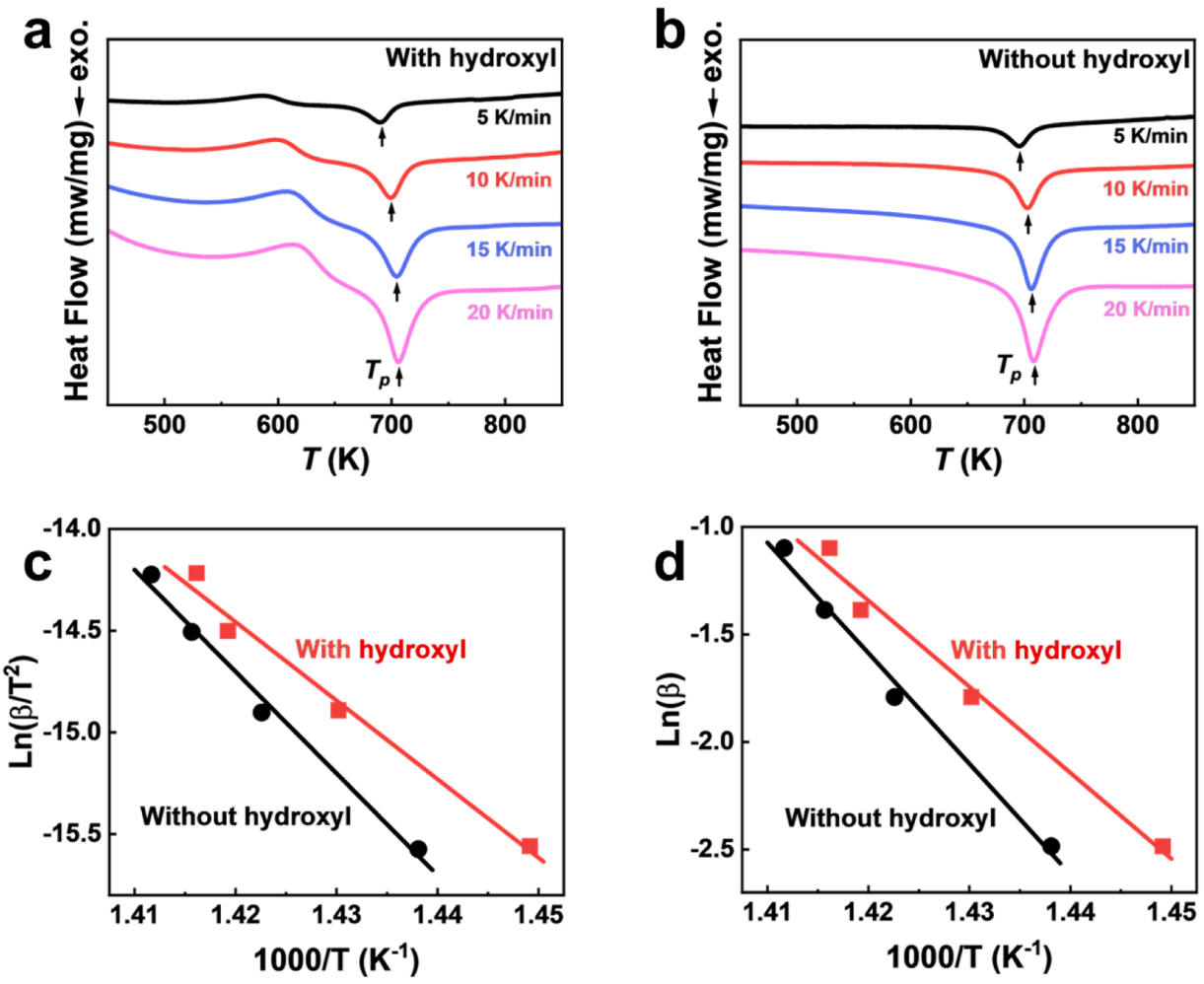

Fig. 5. (a) DSC curves of OH-containing A-TiO_2 at heating rates of 5, 10, 15, and 20 K/min. (b) DSC curves of OH-free A-TiO_2 at heating rates of 5, 10, 15, and 20 K/min. (c) Plots of $1/T_p$ -Ln (β/T_p^2) for both samples: the red curve represents the OH-containing sample, and the black curve corresponds to the OH-free sample. (d) Plots of $1/T_p$-Ln (β) for both samples: the red curve represents the OH-containing sample, and the black curve corresponds to the OH-free sample.

its amorphous structure over this period. The 15-day sample shows a reduced crystallization enthalpy of 147.8 J/g, suggesting that partial crystallization has occurred during this extended storage period. This observation highlights the gradual structural evolution of hydroxyl-containing A-TiO_2 over time. Fig. 3(b) displays the DSC-TG curves of A-TiO_2 heated to 593 K and held for 10 min. Both DSC and TG curves stabilize over time, indicating effective removal of hydroxyl groups during this process. Fig. 3(c) illustrates the DSC curves of hydroxyl-free A-TiO_2 after storage for 10 days and 15 days. The curves (hydroxyl-free sample) lack endothermic peaks, verifying its hydroxyl-free nature. The crystallization enthalpy (Δ_H) value of the as-prepared hydroxyl-free sample is 171.2 J/g, which is comparable to that of the hydroxyl-containing sample. The 10-day sample demonstrates a crystallization enthalpy of 130.6 J/g, which is significantly lower than that of the initial state, indicating that substantial crystallization has already taken place within this timeframe. The 15-day sample further exhibits a reduced crystallization enthalpy of 110.2 J/g, confirming the progression of crystallization over time. These results highlight the relatively lower stability of hydroxyl-free A-TiO_2 compared to its hydroxyl-containing counterpart. Fig. 3(d) compares crystallization enthalpy trends over storage time. Hydroxyl groups enhance the structural stability of A-TiO_2 by forming a hydrogen-bonded network [36], which reduces the mobility of Ti and O atoms and suppresses room-temperature relaxation behavior. Over time, the hydroxyl content gradually decreases. We measured the structural hydroxyl content in freshly prepared samples and samples aged at room temperature for 10 and 15 days, as shown in Fig. S2 (b-d). The results show that the hydroxyl content decreased from 10.8 % to 8.4 % after 15 days of aging. The reduction in hydroxyl content weakens or disrupts the hydrogen-bonded network, leading to increased mobility of Ti and O atoms and gradual crystallization at room temperature. A-TiO_2 without hydroxyl groups, lacking the support of hydrogen bond networks, have a higher rate of Ti and O atomic rearrangement at room temperature than those with hydroxyl groups. Therefore, after 15 days of room-temperature relaxation, hydroxyl-free A-TiO_2 undergo significant crystallization, with a notable decrease in crystallization enthalpy. Interestingly, recent studies have confirmed hydroxyl enrichment in amorphous layers under solar wind H-ion irradiation, which may contribute to the exceptional structural stability of lunar amorphous TiO_2. This provides a basis for the long-term storage of helium-3 in the amorphous layer This finding offers valuable insights for lunar resource utilization, suggesting that hydroxyl groups may play a critical role in stabilizing the amorphous structure of ilmenite surfaces on the Moon.

Figs. 4(a-c) present TEM images of hydroxyl-containing A-TiO_2 after 15 days of ambient storage. The images reveal sporadic lattice fringes, but the amorphous structure remains predominant. The SAED pattern (Fig. 4d) retains diffuse rings typical of amorphous materials, despite minor crystalline regions. In contrast, TEM images of hydroxyl-free A-TiO_2 (Figs. 4e-g) reveal dense and uniformly distributed lattice fringes, confirming significant crystallization. The SAED pattern (Fig. 4h)

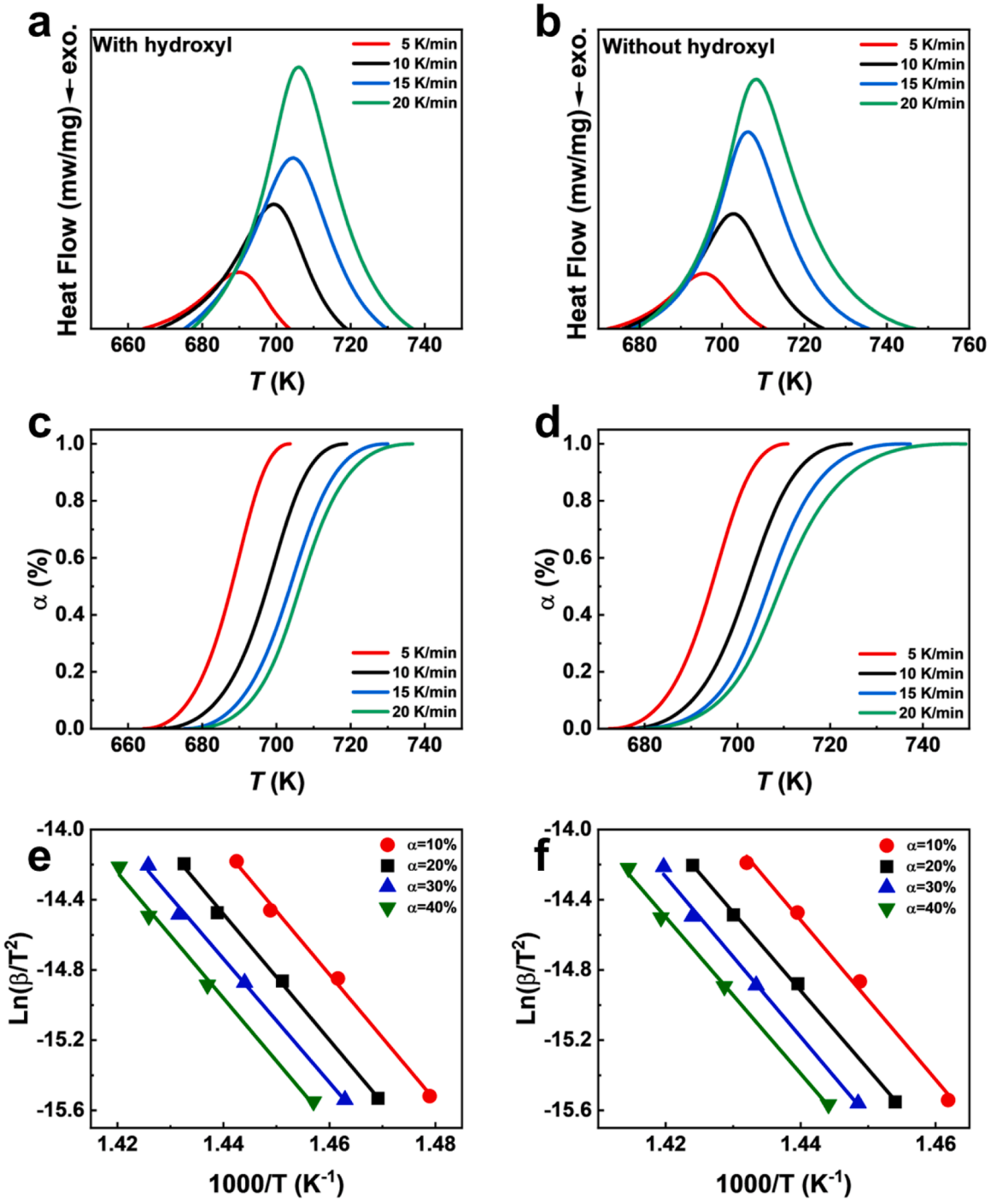

Fig. 6. (a) DSC curves of OH-containing samples at different heating rates. (b) DSC curves of OH-free samples at different heating rates. (c) Degree of crystallization of OH-containing samples, α, as function of temperature at different heating rates. (d) Degree of crystallization of OH-free samples, α, as function of temperature at different heating rates. (e) Plots of $1/T_p$ -Ln (β/T_p^2) for the OH-containing samples. (f) Plots of $1/T_p$ -Ln (β/T_p^2) for the OH-free samples.

exhibits nanocrystalline features, indicating a mixed amorphous-crystalline state. The diffraction pattern identifies the nanocrystalline phase as anatase TiO_2. These TEM results align with crystallization enthalpy data, demonstrating that OH groups effectively enhanced the thermal stability of A-TiO_2.

The non-isothermal crystallization kinetics of the two samples were investigated using TG-DSC at different heating rates. According to the TG-IR and DSC results, the decomposition temperature of the structural hydroxyl groups in the samples ranges from 500 to 650 K, which is lower than the crystallization temperature of A-TiO_2. Consequently, the non-isothermal crystallization test performed on the hydroxyl-containing A-TiO_2 was actually conducted on A-TiO_2 samples where the hydroxyl groups had already been rapidly removed prior to crystallization. Fig. 5 (a) shows the DSC curves of hydroxyl-containing A-TiO_2 at heating rates of 5, 10, 15, and 20 K/min, while Fig. 5(b) presents the corresponding curves for hydroxyl-free samples. Both sets of curves exhibit a shift of crystallization peak temperature to higher values with increasing heating rates, highlighting the kinetic nature of the phase transition. To quantitatively analyze the crystallization kinetics, the activation energy for crystallization was calculated using the Kissinger equation [24,37],

expressed as:

$$\ln\frac{\beta}{T_p^2} = -\frac{E_a}{RT_p} + C \quad (1)$$

where T_p is the peak crystallization temperature in Kelvin (K), β is the heating rate in K/s, E_a is the activation energy in J/mol, R is the universal gas constant (8.314 J/mol·K), and C is a constant. By plotting ln (β/T_p^2) against 1/ T_p and applying the least squares method to fit the data, a linear relationship was obtained. The slope of the fitted line was used to determine the E_a. Figure 5(c) illustrates this linear relationship, demonstrating a strong correlation between the variables.

The calculated activation energy for hydroxyl-containing A-TiO_2 was 321.1 kJ/mol, while that for relaxed hydroxyl-free A-TiO_2 was 415.7 kJ/mol. These results indicate that removal of hydroxyl groups makes A-TiO_2 unstable and prone to crystallization. This could be attributed to the destabilization of the overall structure of A-TiO_2 caused by the breakdown of the hydrogen bond network.

To further validate the reliability of the activation energy values, the Ozawa equation was also employed [38]. The Ozawa equation is given by:

$$\ln(\beta) = -1.0516\frac{E_a}{RT_p} + C \quad (2)$$

the relationship between ln(β) and 1/ T_p, derived from the Ozawa equation, is depicted in Fig. 5(d). By fitting the data and calculating the slope, the crystallization activation energy for hydroxyl-containing A-TiO_2 was determined to be 316.3 kJ/mol, while the hydroxyl-free A-TiO_2 was 406.4 kJ/mol. These values are in close agreement with those obtained from the Kissinger method, confirming the consistency data. We compared our findings with similar studies reported in the literature. In reference [24], two A-TiO_2 samples with differing hydroxyl contents were synthesized. The crystallization activation energy for the sample with higher hydroxyl content was determined to be 276 kJ/mol, while that for the sample with lower hydroxyl content was 356 kJ/mol. These values are in close agreement with our experimental results. The slight discrepancies observed may arise from variations in hydroxyl content attributed to differences in preparation methods.

To further validate the accuracy of our results, we conducted a detailed investigation into the crystallization kinetics of A-TiO_2 using the isoconversional method [39]. As shown in Fig. 6, we calculated the corresponding temperatures when the crystallization fraction α is 10 % to 40 % and determined the crystallization activation energy of the sample through the Kissinger equation. The E_a of samples with hydroxyl groups in the initial state are 299.7 kJ/mol, 298.4 kJ/mol, 292.8 kJ/mol, and 297.3 kJ/mol for 10 %, 20 %, 30 % and 40 % crystallization, respectively. For the samples without hydroxyl group, the E_a are 377.5 kJ/mol, 371.3 kJ/mol, 378.9 kJ/mol, and 370.6 kJ/mol for 10 %, 20 %, 30 % and 40 % crystallization, respectively. Along with the increase of crystallization fraction, the E_a changes <5 %. This is a typical characteristic for allotropic phase transformation that does not involve long-distance atomic diffusion and phase separation. The results show that the E_a values calculated by different methods are close, which also indicates that the rapid decomposition of the hydrogen bond network formed by hydroxyl groups during the heating process reduces the thermal stability of A-TiO_2.

Overall, hydroxyl groups restrict the movement of Ti and O atoms through the formation of hydrogen bond networks, thereby slowing down the room-temperature relaxation behavior of A-TiO_2 and enhancing its thermal stability. Upon continuous heating to the decomposition temperature of hydroxyl groups, the breakdown of the hydrogen bond network introduces structural vacancies, which destabilize the structure of A-TiO_2. This instability facilitates the rearrangement of Ti and O atoms, leading to a reduction in crystallization activation energy. The results highlight the critical influence of hydroxyl groups on the crystallization behavior and activation energy, offering valuable insights into the design and application of A-TiO_2 in fields where thermal stability and phase transformation kinetics are of great importance.

4. Conclusion

A-TiO_2 containing hydroxyl groups, maintaining amorphous structure even after 15 days. In contrast, the crystallization enthalpy of A-TiO_2 samples without hydroxyl decreases from 171.2 J/g to 110.2 J/g after 15 days. Hydroxyl groups enhance the thermal stability of A-TiO_2 by forming hydrogen bond networks. On heating, the hydroxyl-containing A-TiO_2 dehydrate first before crystallization. Such instantaneous A-TiO_2 after dehydration exhibits much lower crystallization activation energy (E_a = 321.1 kJ/mol) than the relaxed hydroxyl-free A-TiO_2 (E_a = 415.7 kJ/mol). The results demonstrate that hydroxyl-containing A-TiO_2 exhibits higher thermal stability. This is a key factor why the amorphous surface layer of lunar ilmenite particles is stable over millions of years.

CRediT authorship contribution statement

Benshun Ma: Writing – original draft, Methodology, Investigation, Formal analysis. **Xiao Chen:** Methodology, Investigation, Formal analysis. **Jianing Wang:** Formal analysis, Data curation. **Wei Xu:** Supervision. **Lijian Song:** Formal analysis, Data curation. **Meng Gao:** Methodology, Formal analysis. **Juntao Huo:** Writing – review & editing, Supervision, Resources, Methodology. **Jun-Qiang Wang:** Writing – review & editing, Supervision, Resources, Methodology, Funding acquisition, Formal analysis, Data curation, Conceptualization.

Declaration of competing interest

The authors declare that they have no known competing financial interests or personal relationships that could have appeared to influence the work reported in this paper.

Acknowledgements

Financial support from the National Natural Science Foundation of China (NSFC U24A201046, 52222105, 51922102), the National Key R&D Program of China (2018YFA0703600), the Youth Innovation Promotion Association CAS (2019296), the Zhejiang Provincial Natural Science Foundation of China (LZ22A030001 and LR22E010004), and the Ningbo 2025 Science and Technology Innovation Project (20212ZDYF020030) is acknowledged.

Supplementary materials

Supplementary material associated with this article can be found, in the online version, at doi:10.1016/j.jnoncrysol.2025.123568.

References

[1] N. Sakai, A. Fujishima, T. Watanabe, K. Hashimoto, Highly hydrophilic surfaces of cathodically polarized amorphous TiO_2 electrodes, J. Electrochem. Soc. 148 (2001) E395.
[2] O. Carp, C.L. Huisman, A. Reller, Photoinduced reactivity of titanium dioxide, Prog. Solid State Chem. 32 (2004) 33–177.
[3] A. Fujishima, K. Honda, Electrochemical photolysis of water at a semiconductor electrode, Nature 238 (1972) 37–38.
[4] Y. Wang, M. Zu, X. Zhou, H. Lin, F. Peng, S. Zhang, Designing efficient TiO_2-based photoelectrocatalysis systems for chemical engineering and sensing, Chem. Eng. J. 381 (2020) 122605.
[5] S. Tian, Y. Feng, Z. Zheng, Z. He, TiO_2-based photocatalytic coatings on glass substrates for environmental applications, Coatings 13 (2023) 1472.
[6] X. Wei, Z. Yang, S.L. Tay, W. Gao, Photocatalytic TiO2 nanoparticles enhanced polymer antimicrobial coating, Appl. Surf. Sci. 290 (2014) 274–279.
[7] W. Hu, H. Liu, H. Hao, Z. Yao, M. Cao, Z. Wang, Z. Song, Influence of TiO_2 additive on the microwave dielectric properties of α-$CaSiO_3$–Al_2O_3 ceramics, Ceram. Int. 41 (2015) S510–S514.

[8] Z. Li, Y. Zhu, L. Wang, J. Wang, Q. Guo, J. Li, A facile method for the structure control of TiO_2 particles at low temperature, Appl. Surf. Sci. 355 (2015) 1051–1056.
[9] J. Pagáčová, A. Plško, K. Michalková, J. Šulcová, B. Bieliková, M. Tomagová, The influence of "small molecules" on properties of TiO_2 films prepared by sol–gel method, J. Non-Cryst. Solids 401 (2014) 164–168.
[10] L. Cui, K. Hui, K. Hui, S. Lee, W. Zhou, Z. Wan, C.-N.H. Thuc, Facile microwave-assisted hydrothermal synthesis of TiO_2 nanotubes, Mater. Lett. 75 (2012) 175–178.
[11] L. Barrientos, P. Allende, M.Á. Laguna-Bercero, J. Pastrián, J. Rodriguez-Becerra, L. Cáceres-Jensen, Controlled Ag-TiO_2 heterojunction obtained by combining physical vapor deposition and bifunctional surface modifiers, J. Phys. Chem. Solids 119 (2018) 147–156.
[12] C. Giolli, F. Borgioli, A. Credi, A. Di Fabio, A. Fossati, M.M. Miranda, S. Parmeggiani, G. Rizzi, A. Scrivani, S. Troglio, Characterization of TiO_2 coatings prepared by a modified electric arc-physical vapour deposition system, Surf. Coat. Technol. 202 (2007) 13–22.
[13] S. Hu, M.R. Shaner, J.A. Beardslee, M. Lichterman, B.S. Brunschwig, N.S. Lewis, Amorphous TiO_2 coatings stabilize Si, GaAs, and GaP photoanodes for efficient water oxidation, Science 344 (2014) 1005–1009.
[14] H. Xiong, M.D. Slater, M. Balasubramanian, C.S. Johnson, T. Rajh, Amorphous TiO_2 nanotube anode for rechargeable sodium ion batteries, J. Phys. Chem. Lett. 2 (2011) 2560–2565.
[15] M.A. Vargas, J.E. Rodríguez-Páez, Amorphous TiO^2 nanoparticles: synthesis and antibacterial capacity, J. Non-Cryst. Solids 459 (2017) 192–205.
[16] Y. Liu, C. Ding, X. Yan, P. Xie, B. Xu, L. Chen, Y. Liu, C. Liu, Y. Yu, Y. Lin, Interface-strain-confined synthesis of amorphous TiO_2 mesoporous nanosheets with stable pseudocapacitive lithium storage, Chem. Eng. J. 420 (2021) 129894.
[17] T. Tarjányi, F. Bogár, J. Minárovits, M. Gajdács, Z. Tóth, Interaction of biomolecules with anatase, rutile and amorphous TiO_2 surfaces: a molecular dynamics study, PLoS ONE 18 (2023) e0289467.
[18] A. Li, X. Chen, L. Song, G. Chen, W. Xu, J. Huo, M. Gao, M. Li, L. Zhang, B. Yao, Taking advantage of glass: capturing and retaining the helium gas on the moon, Mater. Futures 1 (2022) 035101.
[19] Edited by J. Jordan, Mapping pyroclastic deposits and other lunar features for solar wind implanted helium, in: workshop on lunar volcanic glasses: scientific and resource potential. a lunar and planetary institute workshop, sponsored by LPI and the lunar and planetary sample team, held October 10-11, 1989, at the lunar and planetary institute, in Houston, Texas, in: John W. Delano, Grant H. Heiken (Eds.), LPI Technical Report 90-02, published by Lunar and Planetary Institute, LPI Technical Report 90-02, published by Lunar and Planetary Institute, 1990, 3303 NASA Road 1, Houston, TX, 1990, p. 43, 7705843.
[20] G. Kulcinski, H.H. Schmitt, The moon: an abundant source of clean and safe fusion fuel for the 21st century. NASA, Lewis Research Center, Lunar Helium-3 and Fusion Power, 1988.
[21] T. Futagami, M. Ozima, S. Nagal, Y. Aoki, Experiments on thermal release of implanted noble gases from minerals and their implications for noble gases in lunar soil grains, Geochim. Cosmochim. Acta 57 (1993) 3177–3194.
[22] X. Chen, S. Yang, G. Chen, W. Xu, L. Song, A. Li, H. Yin, W. Xia, M. Gao, M. Li, Massive Water Production from Lunar Ilmenite Through Reaction with Endogenous Hydrogen, 5, The Innovation, 2024, p. 5.
[23] M. Abbasi, Y. Dong, J. Meng, D. Morgan, X. Wang, J. Hwang, In situ observation of medium range ordering and crystallization of amorphous TiO_2 ultrathin films grown by atomic layer deposition, APL Mater. 11 (2023) 1.
[24] D. Švadlák, J. Shánělová, J. Málek, L.A. Pérez-Maqueda, J.M. Criado, T. Mitsuhashi, Nanocrystallization of anatase in amorphous TiO_2, Thermochim. Acta 414 (2004) 137–143.
[25] C. Zhou, B. Mo, H. Tang, Y. Gu, X. Li, D. Zhu, W. Yu, J. Liu, Multiple sources of water preserved in impact glasses from Chang'e-5 lunar soil, Sci. Adv. 10 (2024) eadl2413.
[26] M. Hess, C. Wöhler, A.A. Berezhnoy, J.L. Bishop, V.V. Shevchenko, Dependence of the hydration of the lunar surface on the concentrations of TiO_2, Plagioclase, and Spinel, Remote Sens 14 (2021) 47.
[27] Y. Xu, H.-C. Tian, C. Zhang, M. Chaussidon, Y. Lin, J. Hao, R. Li, L. Gu, W. Yang, L. Huang, High abundance of solar wind-derived water in lunar soils from the middle latitude, PNAS 119 (2022) e2214395119.
[28] J. Rasera, J. Cilliers, J. Lamamy, K. Hadler, The beneficiation of lunar regolith for space resource utilisation: a review, Planet. Space Sci. 186 (2020) 104879.
[29] D.C. Hague, M.J. Mayo, Controlling crystallinity during processing of nanocrystalline titania, J. Am. Ceram. Soc. 77 (1994) 1957–1960.
[30] D. Shi, Z. Li, Y. Zhang, X. Kou, L. Wang, J. Wang, J. Li, Synthesis and characterizations of amorphous titania nanoparticles, Nanosci. Nanotechnol. Lett. 1 (2009) 165–170.
[31] X. Chen, S.S. Mao, Titanium dioxide nanomaterials: synthesis, properties, modifications, and applications, Chem. Rev. 107 (2007) 2891–2959.
[32] C.-l. Ma, X.-d. Sun, Synthesis and characterization of amorphous TiO_2 with wormhole-like framework mesostructure, J. Non-Cryst. Solids 319 (2003) 109–116.
[33] J. Soria, J. Sanz, I. Sobrados, J. Coronado, M. Hernández-Alonso, F. Fresno, Water− hydroxyl interactions on small anatase nanoparticles prepared by the hydrothermal route, J. Phys. Chem. C 114 (2010) 16534–16540.
[34] M. Catauro, M. Raucci, F. De Gaetano, A. Marotta, Sol-gel synthesis, characterization and bioactivity of polycaprolactone/SiO_2 hybrid material, J. Mater. Sci. 38 (2003) 3097–3102.
[35] A.A. Magalhães, D.L. Nunes, P.A. Robles-Dutenhefner, E.M. de Sousa, Catalytic activity of porous TiO_2 obtained by sol–gel process in the degradation of phenol, J. Non-Cryst. Solids 348 (2004) 185–189.
[36] N. Saito, M. Akiba, Y. Inagaki, M. Shibata, T. Ishida, H. Kubo, Improved thermal stability of dye-based optical discs: effect of hydrogen bonding, Jpn. J. Appl. Phys. 48 (2009) 042402.
[37] H.E. Kissinger, Reaction kinetics in differential thermal analysis, Anal. Chem. 29 (1957) 1702–1706.
[38] T. Ozawa, Kinetic analysis of derivative curves in thermal analysis, J. Therm. Anal. 2 (1970) 301–324.
[39] H. Minouei, G. Akbari, M. Enayati, S. Hong, Non-isothermal nano-crystallization kinetics in amorphous Ni55Nb35Si10 alloy, Trans. Nonferrous Met. Soc. China 29 (2019) 358–364.